

## FERMI LARGE AREA TELESCOPE DETECTION OF SUPERNOVA REMNANT RCW 86

QIANG YUAN<sup>1,2</sup>, XIAOYUAN HUANG<sup>3</sup>, SIMING LIU<sup>3</sup>, BING ZHANG<sup>2</sup>

<sup>1</sup>Key Laboratory of Particle Astrophysics, Institute of High Energy Physics, Chinese Academy of Sciences, Beijing 100049, China

<sup>2</sup>Department of Physics and Astronomy, University of Nevada Las Vegas, NV 89154, USA

<sup>3</sup>Key Laboratory of Dark Matter and Space Astronomy, Purple Mountain Observatory, Chinese Academy of Sciences, Nanjing 210008, China

*Draft version August 2, 2021*

### ABSTRACT

Using 5.4 year Fermi-LAT data, we report the detection of GeV  $\gamma$ -ray emission from the shell-type supernova remnant RCW 86 (G315.4-2.3) with a significance of  $\sim 5.1\sigma$ . The data slightly favors an extended emission of this supernova remnant. The spectral index of RCW 86 is found to be very hard,  $\Gamma \sim 1.4$ , in the 0.4 to 300 GeV range. A one zone leptonic model can well fit the multi-wavelength data from radio to very high energy  $\gamma$ -rays. The very hard GeV  $\gamma$ -ray spectrum and the inferred low gas density seem to disfavor the hadronic origin of the  $\gamma$ -rays. The  $\gamma$ -ray behavior of RCW 86 is very similar to several other TeV shell-type supernova remnants, e.g., RX J1713.7-3946, RX J0852.0-4622, SN 1006 and HESS J1731-347.

*Subject headings:* radiation mechanisms: non-thermal — gamma rays: ISM — ISM: supernova remnants — cosmic rays

### 1. INTRODUCTION

Supernova remnants (SNRs) are believed to be the most probable candidates of the Galactic cosmic ray (CR) acceleration sources. However, direct observational evidence is not available until there are  $\gamma$ -ray detections of SNRs (e.g., Tavani et al. 2010; Ackermann et al. 2013). Up to now, nearly 20 SNRs have been discovered in TeV  $\gamma$ -ray band, among which 7 are firmly identified as shell-type SNRs (Rieger et al. 2013) and about half are interacting with molecular clouds<sup>1</sup>. In the two-year catalog of Fermi-LAT (2FGL), there are 6 firmly identified SNRs based on the spatial extension and 4 associated point-like SNRs (Nolan et al. 2012). Additionally there are 59 2FGL sources which might be associated with SNRs based on the spatial match between the error circles of 2FGL sources and the SNR extensions (Nolan et al. 2012). With the accumulation of Fermi-LAT data, more and more SNRs were detected (Castro & Slane 2010; Tanaka et al. 2011; Abdo et al. 2011; Wu et al. 2011; Giordano et al. 2012; Ajello et al. 2012; Katsuta et al. 2012; Hewitt et al. 2012; Castro et al. 2013; Araya 2013; Pivato et al. 2013; Xing et al. 2014; Achettil et al. 2014). Although the  $\gamma$ -ray emission mechanism of individual SNRs is subject to debate, it is possible to approach the nature of  $\gamma$ -ray emission of SNRs through a population study with a large sample of  $\gamma$ -ray SNRs (Yuan et al. 2012; Dermer & Powale 2013). Increasing the sample of  $\gamma$ -ray SNRs can be essential for understanding their non-thermal characteristics.

The shell-type SNR G315.4-2.3, also known as RCW 86, is a young remnant probably associated with supernova SN 185 (Stephenson & Green 2002; Zhao et al. 2006). The angular diameter of this SNR is about  $42'$ , with a clear shell in radio (Kesteven & Caswell 1987; Whiteoak & Green 1996; Dickel et al. 2001), infrared (Williams et al. 2011), op-

tical (van den Bergh et al. 1973; Smith 1997) and X-ray bands (Vink et al. 1997; Bocchino et al. 2000; Bamba et al. 2000; Borkowski et al. 2001; Rho et al. 2002). The distance of RCW 86 is estimated to be 2.3 – 2.8 kpc through optical spectroscopy observations (Rosado et al. 1996; Sollerman et al. 2003). In the very high energy (VHE)  $\gamma$ -ray band, a well extended source with morphology consistent with the X-ray image has been revealed by HESS (Aharonian et al. 2009). The spectral index of VHE  $\gamma$ -rays is about 2.5 and the flux is about 10% of that of the Crab nebula (Aharonian et al. 2009). Lemoine-Goumard et al. (2012) analyzed  $\sim 3$  year Fermi-LAT data and found no significant excess from this SNR. Upper limits of  $\gamma$ -ray flux in the GeV band were derived (Lemoine-Goumard et al. 2012). With multi-wavelength observations, the high energy radiation mechanism and particle acceleration can be studied (Aharonian et al. 2009; Lemoine-Goumard et al. 2012).

Here we report the detection of GeV  $\gamma$ -ray emission from RCW 86, with 5.4 year Fermi-LAT data. The data analysis, including the morphology and the spectrum, is presented in Sec. 2. Based on the  $\gamma$ -ray spectrum and the multi-wavelength spectral energy distribution (SED) of RCW 86, we discuss its non-thermal emission mechanism in Sec. 3. Finally Sec. 4 is the conclusion.

### 2. DATA ANALYSIS

The newest reconstructed Pass 7 reprocessed version of the Fermi-LAT data<sup>2</sup> are used in this analysis. We select the data recorded from 4 August 2008 to 16 January 2014, in total 284 weeks. The SOURCE (evclass=2) event class is selected and the maximum zenith angle cut is  $100^\circ$ . The data are filtered with the recommended cuts (DATA\_QUAL==1) && (LAT\_CONFIG==1) && ABS(ROCK\_ANGLE) < 52. The energy range in the analysis is adopted to be 400 MeV to 300 GeV, and the region-of-interest (ROI) is taken to be a  $14^\circ \times 14^\circ$  box around the

<sup>1</sup> <http://tevcat.uchicago.edu>

<sup>2</sup> <http://fermi.gsfc.nasa.gov/ssc/data>

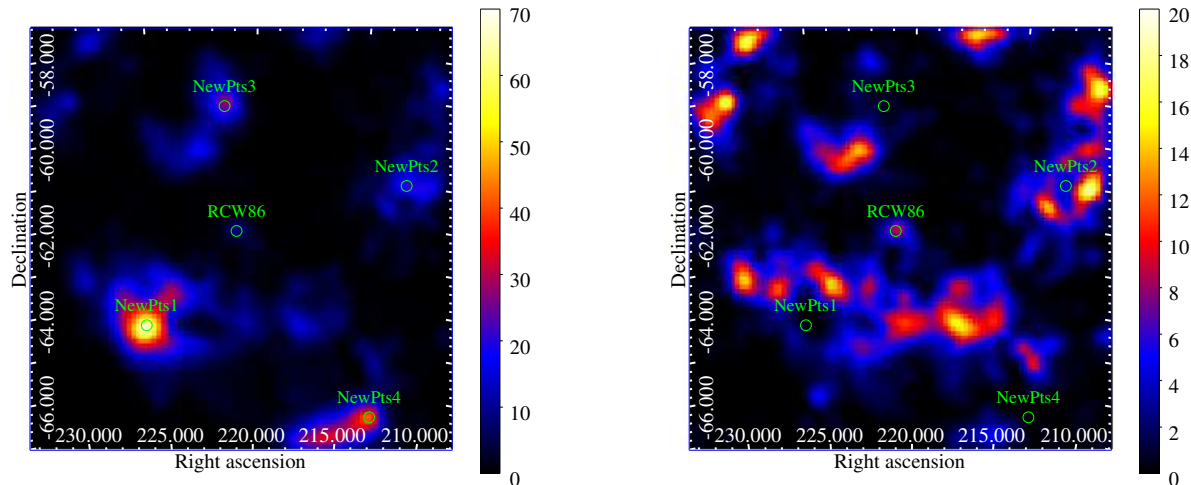


FIG. 1.— TS maps above 400 MeV for  $10^\circ \times 10^\circ$  region centered at RCW 86. Left panel is for the model with the diffuse backgrounds and 2FGL sources subtracted, and the right panel is for the model with the additional sources listed in Table 1 subtracted. Green circles label the positions of the newly added sources and RCW 86. The maps are smoothed with  $\sigma = 0.3^\circ$  Gaussian function.

position of RCW 86. Such a box size is reasonable compared with the  $\lesssim 1.5^\circ$  resolution angle for photons above 400 MeV (Atwood et al. 2009). The analysis is based on the LAT Scientific tool version v9r32p5<sup>3</sup>, and the instrument response function (IRF) is P7REP\_SOURCE\_V15. The Galactic diffuse background g11\_iem\_v05.fits and isotropic diffuse background iso\_source\_v05.txt provided by the Fermi Science Support Center<sup>4</sup> are adopted in the analysis.

We bin the data into 30 logarithmically distributed energy bins and  $140 \times 140$  spatial bins with size  $0.1^\circ$ , and perform the analysis following the standard binned likelihood analysis procedure. The 2FGL sources (Nolan et al. 2012) within radius  $15^\circ$  around RCW 86 are included in the source model, which is generated by the User-contributed software `make2FGLxm1.py`<sup>5</sup>. In the likelihood fittings, the spectral parameters of all the sources located in the ROI together with the normalizations of the two diffuse backgrounds are left free.

We first fit the model with only the 2FGL sources. The Test Statistic (TS, defined as  $2(\ln \mathcal{L} - \ln \mathcal{L}_0)$  with  $\mathcal{L}_0$  the likelihood of null hypothesis and  $\mathcal{L}$  the likelihood with the source included) map for  $10^\circ \times 10^\circ$  region centered at RCW 86 after subtracting this baseline model is shown in the left panel of Fig. 1. The TS map is smoothed with  $\sigma = 0.3^\circ$  Gaussian function. From this TS map we find that there are some excesses which are not included in the 2FGL catalog. We will add five point sources close to the highest TS value locations, whose actual locations will be determined with the `gtfindsrc` tool, to approximate such excess emission (see the green circles in the TS map<sup>6</sup>). At the location of RCW 86 (the center of the map) we see a relatively weak signal which may come from the emission from the SNR. We will also add RCW 86 in the new model. Power law spectra of these newly

added sources are assumed.

The radio and X-ray observations show clear morphology of RCW 86 (Whiteoak & Green 1996; Dickel et al. 2001; Vink et al. 1997; Bocchino et al. 2000; Bamba et al. 2000; Borkowski et al. 2001; Rho et al. 2002), and the angular radius is about  $0.35^\circ$ . The HESS observation of TeV  $\gamma$ -rays reveals the spatial extension with radius of about  $0.4^\circ$  (Aharonian et al. 2009). Therefore RCW 86 should be treated as an extended source in the analysis. We will use a uniform disk with radius  $0.4^\circ$ , the radio image at 843 MHz from the Sydney University Molonglo Sky Survey (SUMSS, Mauch et al. (2003)), and the HESS TeV  $\gamma$ -ray image as the spatial template for RCW 86. The central position of the disk template is adopted to be (R.A. = 220.75, Dec =  $-62.43$ ), which can well match the HESS and SUMSS images of the SNR. The point source assumption will also be adopted for comparison. The three extended spatial templates are shown in Fig. 2. In the left and middle panels the HESS excess contours of  $\gamma$ -rays are overlaid with green lines (Aharonian et al. 2009).

With these new sources in the model, the fitting improves significantly (the value of log-likelihood increases by  $\sim 236$  compared with the fit without these new sources). The coordinates and TS values of the five new point sources are listed in Table 1. The TS map after subtracting the additional five new sources listed in Table 1 is shown in the right panel of Fig. 1. It can be seen that this TS map become much smoother than the baseline model (the left panel). There are still some residual excesses which might be due to the inaccuracy of the Galactic diffuse background or the existence of additional point sources. These residuals are not expected to affect the results of RCW 86 remarkably. Actually even the most significant five new sources listed in Table 1 are not included in the model, the fitting results of RCW 86 do not change significantly.

Now we focus on the discussion about RCW 86. For point source assumption of RCW 86, the best-fit position is RA =  $220.96^\circ$ , Dec =  $-62.32^\circ$ , and the TS value is 26.6. For four degree of freedom (dof) such a TS value corresponds to a significance  $\sim 4.2\sigma$ . As a comparison,

<sup>3</sup> <http://fermi.gsfc.nasa.gov/ssc/data/analysis/software/>

<sup>4</sup> <http://fermi.gsfc.nasa.gov/ssc/data/access/lat/BackgroundModels.html>

<sup>5</sup> <http://fermi.gsfc.nasa.gov/ssc/data/analysis/user/>

<sup>6</sup> The initial postulated position of NewPts 5 is close to NewPts 4. However, the output location from `gtfindsrc` tool is out of the  $10^\circ \times 10^\circ$  region of the TS map.

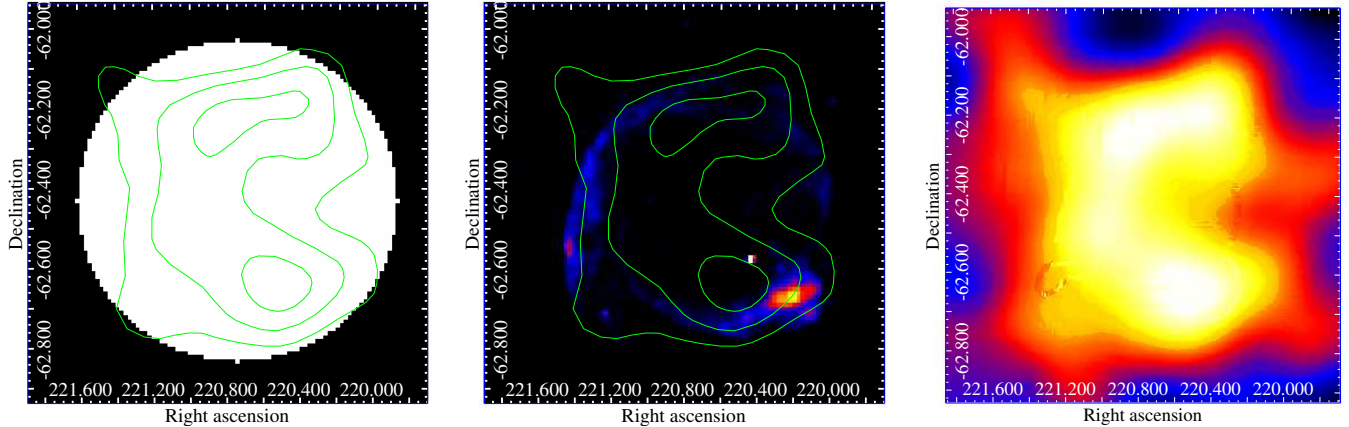


FIG. 2.— Spatial templates used for the analysis. Left: uniform disk with radius  $0.4^\circ$ ; middle: radio image at 843 MHz from SUMSS survey (Mauch et al. 2003); right: HESS image (Aharonian et al. 2009). Green contours overlaid on the left and middle panels are the HESS  $\gamma$ -ray excess contours (Aharonian et al. 2009).

TABLE 1  
COORDINATES AND TS VALUES OF THE NEW POINT SOURCES.

Name	R.A. [deg]	Dec. [deg]	TS
NewPts1	225.91	-64.46	103.7
NewPts2	212.62	-61.00	48.6
NewPts3	221.49	-59.36	51.2
NewPts4	213.08	-66.55	63.6
NewPts5	216.22	-68.15	299.5

in Lemoine-Goumard et al. (2012) the TS value of RCW 86 for point source model is about 12. We then test the three spatial templates as shown in Fig. 2. It is found that for extended source assumption of RCW 86, the TS value is about 30. For two dof (normalization and spectral index) it corresponds to a  $5.1\sigma$  significance. To better address the extension of the source, we compare the results for a disk with very small radius (0.1 degree). The results recover the point source assumption. If the central position of the small disk is the same as the above  $0.4$  deg disk (the best fitting position of point source assumption), the TS value is about 16.9 (28.1). It shows that the data do favor an extended emission of the source. The fitting TS values and spectral indices for different spatial templates are compiled in Table 2. No significant differences among the three spatial templates as shown in Fig. 2 can be found from the Fermi-LAT data.

TABLE 2  
FITTING RESULTS OF DIFFERENT SPATIAL TEMPLATES.

	point	disk	SUMSS	HESS
TS	26.6	32.1	31.6	29.6
$\Gamma$	$1.21 \pm 0.32$	$1.38 \pm 0.18$	$1.36 \pm 0.18$	$1.33 \pm 0.19$
Flux <sup>a</sup>	$2.16 \pm 1.55$	$6.12 \pm 2.95$	$5.66 \pm 2.67$	$5.37 \pm 2.78$

<sup>a</sup>Flux between 0.4 and 300 GeV in  $10^{-10} \text{ cm}^{-2}\text{s}^{-1}$ .

We test different central positions of the disk template through increasing or decreasing the R.A. or Dec. by 0.1 degree. The resulting TS values of RCW 86 decrease by 0.7–4.1. We also test the disk templates with 0.3 and 0.5 degree radii, and get the TS value 30.4 and 29.6 respectively, which are also slightly smaller than the value 32.1 as given in Table 2. It is shown that the disk template shown in Fig. 2 does fit the data well. The best-fitting

spectral indices in these tests differ by about 0.04, which could be regarded as systematics due to the choice of position and extension of the disk.

The spectrum for RCW 86 is very hard. Such a hard spectrum will be difficult to be explained with the hadronic scenario whose  $\gamma$ -ray spectrum just follows the proton spectrum. The inverse Compton scattering of background photons by high energy electrons, on the other hand, can easily account for the hard spectrum revealed by the Fermi-LAT data. Similar hard spectra of GeV photons are also shown in two other shell-type SNRs RX J1713.7-3946 (Abdo et al. 2011) and RX J0852.0-4622 (Tanaka et al. 2011). For another two shell-type SNRs SN 1006 (Araya & Frutos 2012) and HESS J1731-347 (Yang et al. 2014), although they have not been detected yet in Fermi-LAT data, the flux upper limits actually show similar behaviors for the GeV-TeV spectra like RCW 86.

We derive the SED of RCW 86 with the same likelihood analysis, but done in different energy bins. The spectral indices of all the sources are fixed to be the best-fit values obtained in the previous global fitting, only the normalizations of the sources and the diffuse backgrounds are free during the fittings. The SED for the disk template is shown in the left panel of Fig. 3. For the other two extended source templates the results are essentially similar. In the first two energy bins the TS values for RCW 86 are very small, and the 99.9% upper limits are given. For comparison the upper limits obtained in Lemoine-Goumard et al. (2012) and the HESS data in the VHE band (Aharonian et al. 2009) are also shown. The GeV  $\gamma$ -ray SED derived in this work is consistent with the upper limits obtained in Lemoine-Goumard et al. (2012). It can be seen that connecting the GeV-TeV SED shows a peak at hundreds of GeV. Such a peak may indicate the leptonic feature of the  $\gamma$ -ray emission.

### 3. DISCUSSION

In the right panel of Fig. 3 we compile the multi-wavelength observational data of RCW 86, from radio (Caswell et al. 1975), X-ray (Lemoine-Goumard et al. 2012), to VHE  $\gamma$ -rays (Aharonian et al. 2009). This wide band SED shows a double-peak behavior, which



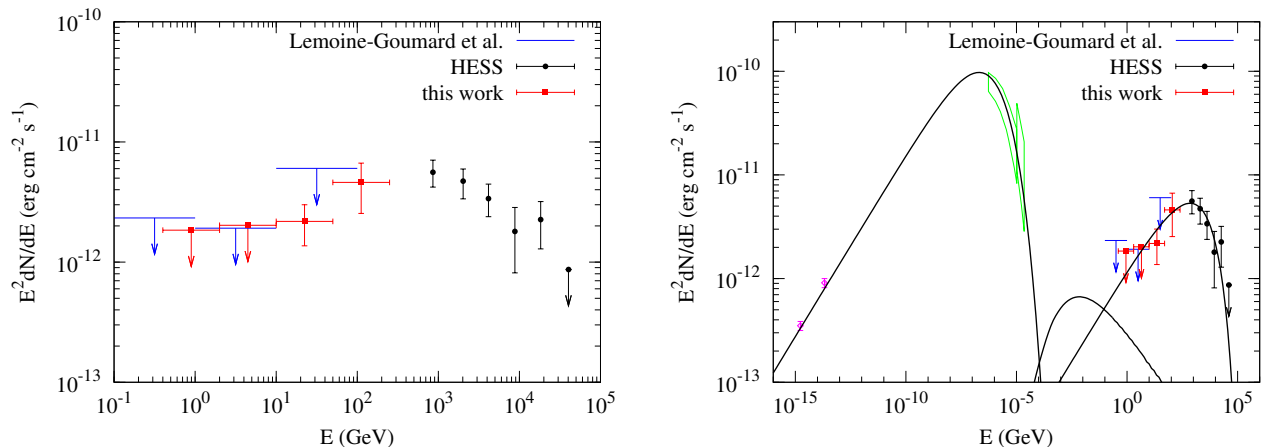


FIG. 3.— Left:  $\gamma$ -ray spectrum of RCW 86 for the disk template. Black dots are the HESS data in the VHE band (Aharonian et al. 2009), and blue arrows are the upper limits derived using 40 month Fermi data (Lemoine-Goumard et al. 2012). Right: multi-wavelength SED of RCW 86. Radio data are from Molongo at 408 MHz and Parkes at 5 GHz (Caswell et al. 1975); X-ray data from ASCA and RXTE (Lemoine-Goumard et al. 2012). Lines show a one-zone leptonic modeling of the data, with the three bumps from left to right synchrotron, bremsstrahlung and inverse Compton scattering components respectively.

might be reasonably described within the leptonic framework. The high energy electron spectrum is parameterized with an exponential cutoff power-law spectrum,  $dN/dE_e \propto E_e^{-\Gamma_e} \exp(-E_e/E_c)$ . The total energy of electrons above 1 GeV is normalized to  $W_e$ , which could be a fraction of the total energy released by the supernova. We consider a simple one zone model, where a single electron population radiates in a uniform magnetic field and matter field. For the background photons used to calculate the inverse Compton scattering emission, we adopt the interstellar radiation field (ISRF) as developed in Porter & Strong (2005), which is made up of optical emission from starlight, infrared from absorption and re-emission from dust and the cosmic microwave background (CMB). To calculate the bremsstrahlung emission, we also adopt a gas number density of  $1 \text{ cm}^{-3}$ . Adopting proper parameters, we reproduce the multi-wavelength emission of RCW 86 well, as shown in the right panel of Fig. 3. The three bumps from left to right represent the synchrotron, bremsstrahlung and inverse Compton scattering components generated by the same population of electrons. Although the radio and X-ray images show complex structures, the gamma-ray observations are fully consistent with the one-zone model. The X-ray emission has contributions from a thermal component, and the synchrotron emission is also affected by the magnetic field structure. There is no compelling evidence for a two-zone emission model.

Assuming that the distance of RCW 86 is 2.5 kpc, and the radius is 15 pc, we estimate the model parameters to reproduce the multi-wavelength SED, which are  $\Gamma_e \approx 2.3$ ,  $E_c \approx 22 \text{ TeV}$ ,  $W_e \approx 1.2 \times 10^{48} \text{ erg}$ , and  $B \approx 20 \mu\text{G}$ . These parameters are consistent with<sup>7</sup> that of the one zone model in Lemoine-Goumard et al. (2012). The total energy goes to high energy electrons is about 0.1% of the typical released energy of a supernova, say  $10^{51} \text{ erg}$ . We also test the case with only the CMB as the target photon field to produce the inverse Compton scattering emission. In this case, the total energy of electrons ( $W_e$ )

needs to be  $\sim 2$  times higher, the magnetic field is about  $\sqrt{2}$  times smaller, and the cutoff energy  $E_c \approx 26 \text{ TeV}$  which is slightly larger. The resulting photon spectrum for the CMB photon field case is very similar as the one shown in the right panel of Fig. 3.

It should be noted that the cooling of electrons is not effective enough to alter the electron spectrum of RCW 86. From Fig. 3 we see that most of the electron energy goes into synchrotron radiation. The synchrotron cooling time is estimated as  $\tau_{\text{syn}} \approx 1.25 \times 10^{10} (B/\mu\text{G})^{-2} (E/\text{GeV})^{-1} \text{ yr}$ . The age of RCW 86 is about 1800 yr, thus the critical energy above which the electrons are cooled down is about 35 (17) TeV for magnetic field 14 (20)  $\mu\text{G}$ . Since our cutoff energy is about 20 TeV, the cooling does not affect the electron spectrum assumed in the modeling.

The hadronic scenario seems not favored to explain the  $\gamma$ -ray spectrum since it requires too hard a spectrum of the accelerated cosmic ray protons, which can not be easily understood in the shock acceleration theory. There might be another problem for the hadronic scenario, which is the low ambient medium density as revealed by the thermal X-ray emission. In the above calculation we arbitrarily adopt a gas density of  $1 \text{ cm}^{-3}$ . From the weak thermal X-ray emission, the post-shock density of this SNR was estimated to be  $(0.26-0.68) f^{-0.5} \text{ cm}^{-3}$ , where  $f$  is the filling factor of the thermal component (Yamaguchi et al. 2008). A low density is also expected according to the high shock velocity of this SNR (Helder et al. 2009). Given a low density, the required energy for proton acceleration will be too high. For example, for the proton spectrum with index 1.7 and cutoff energy 50 TeV, the estimated total energy above 1 GeV is  $1.3 \times 10^{50} (n_{\text{gas}}/1 \text{ cm}^{-3})^{-1} (d/2.5 \text{ kpc})^2 \text{ erg}$ . The energy fraction of cosmic rays in the total energy released by the supernova may be too large if the density is lower than  $1 \text{ cm}^{-3}$ . In a recent study, Morlino et al. (2013) inferred the cosmic ray acceleration efficiency would be  $\sim 20\%$  based on the Balmer line emission. Therefore the energy budget will be challenged in the hadronic scenario. Similar circumstances also appear for SNR RX

<sup>7</sup> Except for  $W_e$  which might be due to different low threshold energy to calculate the total electron energy.

J1713.7-3946 (Ellison et al. 2010; Yuan et al. 2011) and RX J0852.0-4622 (Tanaka et al. 2011), both having very hard GeV  $\gamma$ -ray spectra and no detection of thermal X-rays. Note Fang et al. (2011) proposed the hadronic scenario based on non linear diffusive shock acceleration (Malkov & O’C Drury 2001; Blasi 2002) to explain the  $\gamma$ -ray emission of these three SNRs. The model prediction is generally higher and harder than the Fermi-LAT observations.

The GeV-TeV  $\gamma$ -ray emission of this SNR, together with the fact that the ambient medium density may be low, further supports the unified picture to describe the  $\gamma$ -ray SNRs (Yuan et al. 2012). In that model, the SNRs are classified into three classes according to the medium density. The sources located in low density medium tend to have an inverse Compton scattering origin of  $\gamma$ -rays, and the  $\gamma$ -ray spectrum will be very hard. Up to now, there are probably five shell-type SNRs belong to this class, i.e., RX J1713.7-0846, RX J0852.0-4622, RCW 86, SN 1006 and HESS J1731-347. A combined study of all these sources and an evolutionary picture to describe them will be interesting.

#### 4. CONCLUSION

In this work we report the detection of GeV  $\gamma$ -rays from a shell-type SNR RCW 86 with Fermi-LAT. Analyzing 5.4 year Fermi-LAT data, we find an extended source

coincident with the radio or VHE  $\gamma$ -ray image of RCW 86 with a significance higher than  $5\sigma$ . The point source assumption is less favored than the extended source assumption. The GeV  $\gamma$ -ray spectrum is found to be very hard,  $\Gamma \approx 1.4 \pm 0.2$ . The multi-wavelength SED from radio to VHE  $\gamma$ -rays can be well described with a simple one zone leptonic model. The hadronic scenario may face difficulty in producing the very hard GeV  $\gamma$ -ray spectrum and in the total energy budget given that the environmental medium density is relatively low. The analogy of the non-thermal GeV-TeV spectrum and the lack of strong thermal X-ray emission of this SNR with several other shell-type SNRs makes them form a distinct class of  $\gamma$ -ray SNRs, which may point to the nature of the particle acceleration and radiation in SNRs.

#### ACKNOWLEDGEMENTS

We acknowledge the use of the Fermi-LAT data provided by the Fermi Science Support Center, and the anonymous referee for useful comments and suggestions. QY thanks Ye Li for helpful discussion. This work is supported by 973 Program under Grant No. 2013CB837000, the National Natural Science Foundation of China under Grant Nos. 11105155, 11173064 and 11233001, and the Strategic Priority Research Program – The Emergence of Cosmological Structures of the Chinese Academy of Sciences under Grant No. XDB09000000.

#### REFERENCES

- Abdo, A. A., et al. 2011, *ApJ*, 734, 28  
 Ackermann, M., et al. 2013, *Science*, 339, 807  
 Aharonian, F., et al. 2009, *ApJ*, 692, 1500  
 Ajello, M., et al. 2012, *ApJ*, 744, 80  
 Araya, M. 2013, *MNRAS*, 434, 2202  
 Araya, M., & Frutos, F. 2012, *MNRAS*, 425, 2810  
 Atwood, W. B., et al. 2009, *ApJ*, 697, 1071  
 Auchettl, K., Slane, P., & Castro, D. 2014, *ApJ*, 783, 32  
 Bamba, A., Koyama, K., & Tomida, H. 2000, *PASJ*, 52, 1157  
 Blasi, P. 2002, *Astroparticle Physics*, 16, 429  
 Bocchino, F., Vink, J., Favata, F., Maggio, A., & Sciortino, S. 2000, *A&A*, 360, 671  
 Borkowski, K. J., Rho, J., Reynolds, S. P., & Dyer, K. K. 2001, *ApJ*, 550, 334  
 Castro, D., & Slane, P. 2010, *ApJ*, 717, 372  
 Castro, D., Slane, P., Carlton, A., & Figueroa-Feliciano, E. 2013, *ApJ*, 774, 36  
 Caswell, J. L., Clark, D. H., & Crawford, D. F. 1975, *Australian Journal of Physics Astrophysical Supplement*, 37, 39  
 Dermer, C. D., & Powale, G. 2013, *A&A*, 553, A34  
 Dickel, J. R., Strom, R. G., & Milne, D. K. 2001, *ApJ*, 546, 447  
 Ellison, D. C., Patnaude, D. J., Slane, P., & Raymond, J. 2010, *ApJ*, 712, 287  
 Fang, J., Tang, Y., & Zhang, L. 2011, *ApJ*, 731, 32  
 Giordano, F., et al. 2012, *ApJ*, 744, L2  
 Helder, E. A., et al. 2009, *Science*, 325, 719  
 Hewitt, J. W., Grondin, M.-H., Lemoine-Goumard, M., Reposeur, T., Ballet, J., & Tanaka, T. 2012, *ApJ*, 759, 89  
 Katsuta, J., et al. 2012, *ApJ*, 752, 135  
 Kesteven, M. J., & Caswell, J. L. 1987, *A&A*, 183, 118  
 Lemoine-Goumard, M., Renaud, M., Vink, J., Allen, G. E., Bamba, A., Giordano, F., & Uchiyama, Y. 2012, *A&A*, 545, A28  
 Malkov, M. A., & O’C Drury, L. 2001, *Reports of Progress in Physics*, 64, 429  
 Mauch, T., Murphy, T., Buttery, H. J., Curran, J., Hunstead, R. W., Piestrzynski, B., Robertson, J. G., & Sadler, E. M. 2003, *MNRAS*, 342, 1117  
 Morlino, G., Blasi, P., Bandiera, R., & Amato, E. 2013, *A&A*, 562, A141  
 Nolan, P. L., et al. 2012, *ApJS*, 199, 31  
 Pivato, G., et al. 2013, *ApJ*, 779, 179  
 Porter, T. A., & Strong, A. W. 2005, *International Cosmic Ray Conference*, 4, 77  
 Rho, J., Dyer, K. K., Borkowski, K. J., & Reynolds, S. P. 2002, *ApJ*, 581, 1116  
 Rieger, F. M., de Oña-Wilhelmi, E., & Aharonian, F. A. 2013, *Frontiers of Physics*, 8, 714  
 Rosado, M., Ambrocio-Cruz, P., Le Coarer, E., & Marcelin, M. 1996, *A&A*, 315, 243  
 Smith, R. C. 1997, *AJ*, 114, 2664  
 Sollerman, J., Ghavamian, P., Lundqvist, P., & Smith, R. C. 2003, *A&A*, 407, 249  
 Stephenson, F. R., & Green, D. A. 2002, *Historical supernovae and their remnants*, by F. Richard Stephenson and David A. Green. *International series in astronomy and astrophysics*, vol. 5. Oxford: Clarendon Press, 2002, ISBN 0198507666, 5  
 Tanaka, T., et al. 2011, *ApJ*, 740, L51  
 Tavani, M., et al. 2010, *ApJ*, 710, L151  
 van den Bergh, S., Marscher, A. P., & Terzian, Y. 1973, *ApJS*, 26, 19  
 Vink, J., Kaastra, J. S., & Bleeker, J. A. M. 1997, *A&A*, 328, 628  
 Whiteoak, J. B. Z., & Green, A. J. 1996, *A&AS*, 118, 329  
 Williams, B. J., et al. 2011, *ApJ*, 741, 96  
 Wu, J. H. K., Wu, E. M. H., Hui, C. Y., Tam, P. H. T., Huang, R. H. H., Kong, A. K. H., & Cheng, K. S. 2011, *ApJ*, 740, L12  
 Xing, Y., Wang, Z., Zhang, X., & Chen, Y. 2014, *ApJ*, 781, 64  
 Yamaguchi, H., Koyama, K., Nakajima, H., Bamba, A., Yamazaki, R., Vink, J., & Kawachi, A. 2008, *PASJ*, 60, 123  
 Yang, R.-z., Zhang, X., Yuan, Q., & Liu, S. 2014, *ArXiv e-prints*:1405.4888  
 Yuan, Q., Liu, S., & Bi, X. 2012, *ApJ*, 761, 133  
 Yuan, Q., Liu, S., Fan, Z., Bi, X., & Fryer, C. L. 2011, *ApJ*, 735, 120  
 Zhao, F.-Y., Strom, R. G., & Jiang, S.-Y. 2006, *Chin. J. Astron. Astrophys.*, 6, 635